Rockburst time warning method with blasting cycle as the unit based on microseismic information time series: a case study

Lei Hu[1,2] · Xia-Ting Feng[1,2] · Zhi-Bin Yao[1,2] · Wei Zhang[1,2] · Wen-Jing Niu[1,2] · Xin Bi[1,2] · Guang-Liang Feng[3] ·
Ya-Xun Xiao[3]

Abstract

Rockburst warning includes prediction of the position, intensity, and timing of potential rockburst. Rockburst time warning refers to the prediction of the moment at or time period during which a rockburst may occur. Due to the complex rockburst mechanism and many influencing factors, several key difficult-to-solve scientific problems currently remain in rockburst time warning research. In this article, microseismic (MS) monitoring is performed, and blasting is implemented as an iconic event to study the warning method for rockburst with blasting cycle as the unit of time. Focusing on this research goal, a deep learning method is applied to establish an MS information prediction model (MSIPM) and a rockburst time warning model (RBTWM) based on a long short-term memory network (LSTM). The MSIPM predicts the MS information for subsequent blasting cycles through the MS information time series of historical blasting cycles. The RBTWM predicts the potential rockburst intensity and which blasting cycle a rockburst may occur through the MS information time series obtained by fusing MS information from historical and subsequent blasting cycles. The developed method is applied in a railway tunnel excavated with the drilling and blasting method. The warning results of the test set demonstrate that the rockburst warning accuracies for the first, second, and third subsequent blasting cycles are approximately 74.6%, 71.2%, and 63.1%, respectively. In addition, further application and verification are carried out in the construction of another new railway tunnel. The rockburst warning accuracy for the first subsequent blasting cycles is approximately 80.0%. The application results show that the MSIPM and RBTWM provide warnings regarding the immediate rockburst time in blasting cycle units. The combination of MS monitoring and artificial intelligence represents a new idea for rockburst time warning.

Keywords Rockburst · Microseismic monitoring · Rockburst time warning · Deep tunnel · Deep learning

Introduction

Rockburst is a dynamic phenomenon involving the violent failure and ejection of surrounding rock caused by the sudden release of the elastic potential energy of deformation accumulated in underground engineering rock masses during excavation or due to other disturbances (Feng et al. 2022; Gong et al. 2019a). Rockbursts may cause human casualties, economic losses, and delays in construction periods. As human engineering activities reach increasingly deeper locations underground, the geological environments of underground engineering are becoming increasingly complex, the ground stress level is increasing, and the problem of rockburst disasters induced by excavation is becoming much more prominent. Rockbursts have occurred in underground mines, underground hydropower stations, underground military facilities, and underground transportation tunnels in many countries (Ortlepp 2005; Stacey 2013; Meng et al. 2017; Zhou et al. 2018; Hu et al. 2019, 2020). Obviously, rockburst has become one of the bottleneck problems restricting the safe construction of deep rock masses. Tunnels are ubiquitous in underground engineering, and during the construction of deep tunnels in hard rock, the drilling and blasting (D&B) method is a widely applied method,

✉ Lei Hu
  hulei@mail.neu.edu.cn

[1] Key Laboratory of Ministry of Education on Safe
  Mining of Deep Metal Mines, Northeastern University,
  Shenyang 110819, China

[2] Key Laboratory of Liaoning Province on Deep Engineering
  and Intelligent Technology, Northeastern University,
  Shenyang 110819, China

[3] State Key Laboratory of Geomechanics and Geotechnical
  Engineering, Institute of Rock and Soil Mechanics, Chinese
  Academy of Sciences, Wuhan 430071, China

while immediate rockburst is a relatively frequent rockburst type in these tunnels (Feng et al. 2019a). Therefore, research on warning methods for immediate rockburst is of great significance to reduce the risk of engineering accidents caused by rockburst.

In recent decades, experts and scholars have proposed numerous methods for rockburst evaluation and warning. These methods can be mainly divided into geological analysis methods (Li et al. 2017), empirical methods (Hoek and Brown 1980; Singh 1987; Wang and Park 2001; Mitri 2007; Chen et al. 2009; Zhao et al. 2017; Liu et al. 2023), numerical simulation analysis methods (Zubelewicz and Mroz 1983; Müller 1991; Jiang et al. 2010; Zhu et al. 2010; Hatzor et al. 2017), laboratory rock mechanics experiment methods (Jiang et al. 2021; Zhang et al. 2019; Gong et al. 2019b), physical modeling experiment methods (Vacek and Chocholoušová 2008; Lu et al. 2018), neural network methods (Zhou and Gu 2004; Shi et al. 2010; Faradonbeh and Taheri 2019), and on-site monitoring methods (Mendecki 1993; Fajklewicz 2006; Zhao et al. 2014; Feng et al. 2015a; Xiao et al. 2016; Li et al. 2016; He et al. 2019; Liu et al. 2021; Guo et al. 2022). Among the on-site monitoring methods, the microseismic (MS) monitoring method has been widely applied in the construction phase of a project due to its relatively high accuracy. Moreover, at present, the rockburst warning method based on MS monitoring is relatively accurate in predicting the position and intensity of potential rockbursts, while the time of a potential rockburst can only be approximated and the warning result can only be given in terms of a long period due to the complex rockburst mechanism and its many influencing factors. This makes it difficult to accurately determine the timing of rockburst prevention and control measures, making the prevention and control effects unsatisfactory. Therefore, further rockburst time warning research is urgently needed. Rockburst time warnings can be divided into narrow- and broad-sense warnings. The narrow sense of a rockburst time warning refers to the prediction of the moment of a potential rockburst. The broad sense of a rockburst time warning refers to the prediction of the time period during which a rockburst may occur. This time period can be a day, a construction cycle or a construction step, etc. At present, it is not realistic to address the narrow sense of rockburst time warning due to the limited technical means and limited understanding of the rockburst mechanism. Therefore, this paper mainly examines the method of broad-sense rockburst time warning.

Previous research results have demonstrated that blasting exerts a great impact on immediate rockburst in terms of both the rockburst occurrence area and rockburst occurrence time in tunnels excavated by the D&B method. The specific manifestations are as follows: immediate rockburst mostly occurs near the working face and within a few hours after the most recent blasting. The microseismicity observed in the development process of immediate rockburst is also closely related

to the blasting of the working face (Hu et al. 2020; Liu et al. 2013). Regardless of the MS event number, energy, or apparent volume, microseismicity largely remains active within a few hours after blasting and is mainly distributed near the working face (Hu et al. 2019, 2020; Feng et al. 2015a). This indicates that blasting, microseismicity and rockburst are closely related in time, space, and intensity. Therefore, it is feasible to split MS information according to the blasting cycle (the time period between two adjacent blasts on the working face) and to use blasting to couple MS information with rockbursts to develop a warning method for the immediate rockburst time, taking the blasting cycle as the unit.

The MS information in the development process of a rockburst constitutes a time series, and the key to immediate rockburst time warning is to determine the deep features of the MS information time series. The rapid development of artificial intelligence has yielded strong learning and prediction capabilities in many fields (LeCun et al. 2015; Granter et al. 2017). Therefore, artificial intelligence has been introduced in rockburst MS monitoring and prediction. Huang et al. (2018) used convolutional neural networks and deep learning techniques to develop a method for identifying the time delay of arrival and subsequently the source location of MS events in underground mines. Zhang et al. (2021) designed a U-Net neural network to automatically detect the P- and S-wave arrival times of MS waveforms in tunnels to realize automatic MS monitoring. Pu et al. (2019) employed a support vector classifier to predict rockburst in kimberlite pipes at a diamond mine. Luis et al. (2017) used different data mining techniques ranging from artificial neural networks to naive Bayesian classifiers to build models to predict rockbursts. Therefore, this paper adopts artificial intelligence to establish an MS information prediction model (MSIPM) and rockburst time warning model (RBTWM) to realize a warning method for immediate rockburst time, taking the blasting cycle as the unit.

# Engineering background

Project description

The tunnel studied in this paper is located in southwest China. The length of the tunnel is approximately 13 km, the maximum burial depth is approximately 2 km, the section shape is a city gate type, and the section size is 7.2 m × 6.2 m (width × height), as shown in Fig. 1 (Hu et al. 2020). The tunnel was mainly excavated in whole sections using the D&B method, with an average excavation step length of 3.2 m. The main support mode used in the tunnel is a thin layer of shotcrete. In addition, in sections where the geological condition is very poor or rockburst has occurred, steel arches, rockbolts, or steel mesh are added, as required.
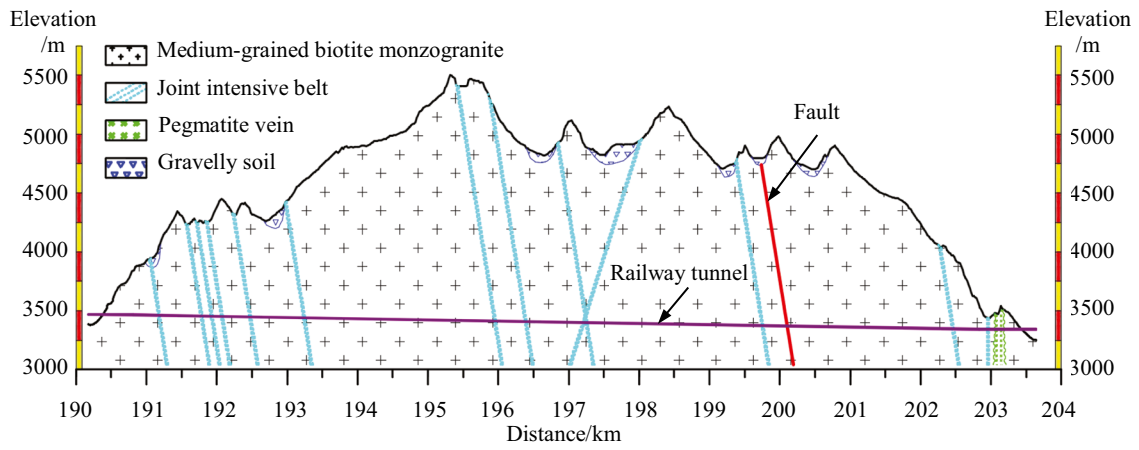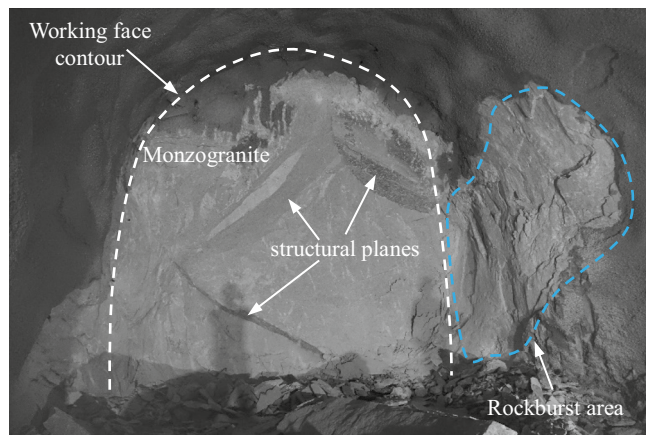
(a) A vertical cross section along the tunnels detailing their geology
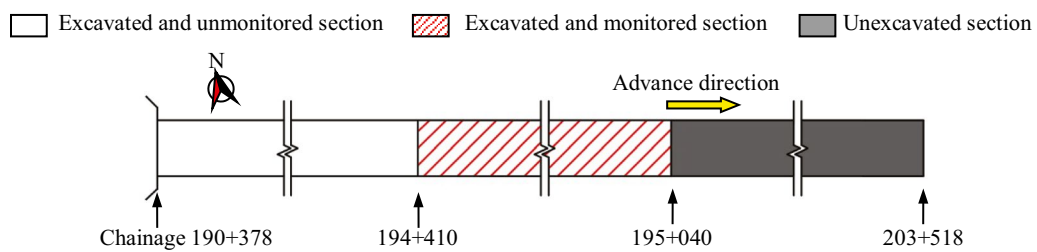
(b) A plane view of the tunnel highlighting the distribution of the MS monitoring sections (up to July 31, 2017)
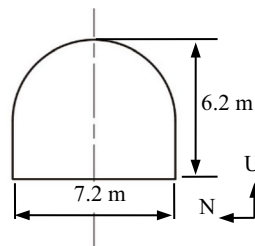
(c) A vertical cross section perpendicular to the axis of the tunnel

(d) A photograph of typical geological conditions near the working face of the tunnel

Fig. 1 Layout and geological conditions of the railway tunnel located in Southwest China (Hu et al. 2020)

Geological conditions

The rock layer through which the tunnel passes is largely composed of granite from the Tertiary Eocene (E^2R). In situ stress test results indicate that the maximum, intermediate, and minimum principal stresses in the tunnel engineering area are approximately 50, 37, and 36 MPa, respectively, and the maximum principal stress is the near-horizontal stress dipping slightly to the NNE direction (Hu et al. 2020).

Rockburst MS monitoring in the tunnel

The tunnel has been plagued by rockbursts since its excavation. To reduce the loss caused by rockbursts, our team established a high-performance MS monitoring system in the tunnel to monitor and warn of potential rockburst disasters during the tunnel construction. Detailed information has been provided in related papers (Hu et al. 2020; Feng et al. 2019a).

Basic process and framework of the warning method

It is necessary to classify rockbursts according to a unified standard when a database of rockburst cases has been established and a rockburst warning is actually issued. Feng et al. (2019b) classified rockbursts into slight, moderate, intense, and extremely intense rockbursts according to the harmfulness, failure depth, failure length along the tunnel axis, average initial ejection velocity of the rockburst block, characteristics of the rockburst block, and sound. The above four rockburst intensities are mainly considered in this paper.

The basic idea of the warning method for the immediate rockburst time in a tunnel excavated by the D&B method is as follows: selecting the time series of MS information of historical blasting cycles in the warning area as samples, then mining the deep characteristics of MS information evolution with the blasting cycle by the deep learning method, and ultimately establishing the MSIPM based on the long short-term memory network (LSTM). In addition, choosing the actual rockburst situation of each blasting cycle and the time series composed of the MS information of each blasting cycle as samples, the nonlinear relationship between rockburst and MS information time series is mined by the deep learning method, and the RBTWM based on LSTM is created. In actual rockburst warnings, the MSIPM is used to predict the MS information of subsequent blasting cycles. The MS information of historical blasting cycles is then fused with the predicted MS information of the subsequent blasting cycle. The time series formed by the fused MS information is thereafter substituted into the RBTWM, and the intensity of a potential rockburst in the subsequent

blasting cycle is output after calculation. This achieves the warning of the immediate rockburst time taking the blasting cycle as the unit. The basic flow of the warning method is shown in Fig. 2.

Pretreatment of the MS monitoring data

Warning unit

The rockburst warning unit is determined by the spatial scope and time span, as shown in Fig. 3. Feng et al. (2015a) and Martin (1997) studied the spatial scope of warning units by considering many factors. According to their research results, the combined effect of the factors can be uniformly characterized by the equivalent diameter of the tunnel. In particular, the spatial scope of the warning unit along the tunnel axis ranges from approximately 3.5 times the equivalent diameter behind the working face to 1.5 times the equivalent diameter in front of the working face, and the spatial scope along the radial direction of the tunnel is approximately 10 times the equivalent diameter of the tunnel. The spatial scope of the warning unit is calculated by Eq. (1):

$$\begin{cases} x \in \left[-3.5D_e, +1.5D_e\right] \\ y \in \left[-5D_e, +5D_e\right] \\ z \in \left[-5D_e, +5D_e\right] \end{cases} \tag{1}$$

where x is the distribution range of the warning unit along the axis of the tunnel, "+" indicates the front of the working face, "−" indicates the rear of the working face, y is the distribution range of the warning units in the horizontal plane perpendicular to the tunnel axis direction, "+" indicates the positive direction of the y-axis, "−" indicates the negative direction of the y-axis, z is the distribution range of the warning units in the vertical direction, "+" indicates the vertical upward direction, "−" indicates the vertical downward direction, and De is the average equivalent diameter of the monitoring section of the tunnel.

In general, the time span of the warning unit should include the entire development process of rockburst; the time span should range from the moment when the first MS event occurs in the spatial scope of the warning unit to the moment before rockburst occurs. However, because the research goal of this paper is to provide a warning of the immediate rockburst time, taking the blasting cycle as the unit, a rockburst will have not yet occurred when a warning is issued, and the exact moment immediately before rockburst cannot be determined. Therefore, the time span of the warning units considered in this paper ranges from the moment of the first blasting to the moment of the most recent blasting in the spatial scope of the warning unit.

Fig. 2 Basic flow of the warning method of rockburst time, taking the ▶ blasting cycle as the unit

During tunnel excavation, the working face advances. On the basis of maintaining the same size, the spatial scope of the warning unit needs to advance along the tunnel axis. The time span of the warning unit also needs to be adjusted with the implementation of blasting at the working face.

Treatment of the blasting cycle

Because the research goal of this paper is to realize the immediate rockburst time warning taking the blasting cycle as a unit, it is necessary to discretize the MS data obtained by the MS monitoring system in blasting cycle units when establishing MS information time series samples. When discretizing the MS data by the blasting cycle, the following two problems should be considered: the unification of the blasting cycle length and the replacement of missing MS information.

### Unification of the blasting cycle length

In a tunnel project, the duration of each blasting cycle does not remain completely constant. When establishing MS information time series samples, if the relevant MS information is directly calculated according to the actual duration of each blasting cycle, the prediction effect of the model trained by these samples could be adversely affected, so it is necessary to unify the duration of each blasting cycle to a fixed length.

In a blasting cycle, the microseismicity gradually increases after blasting, reaches its peak after several hours, and then gradually decreases. Therefore, the unified blasting cycle length should still include the whole process of microseismicity increase and the main process of microseismicity decline to ensure that the main microseismicity features produced during each blasting cycle participate in prediction model training and are characterized in the subsequent prediction steps.

Although the blasting cycle duration does not necessarily remain constant throughout the entire tunnel project, generally, it exhibits little difference and the degree of dispersion is low (as shown in Fig. 4). Therefore, the length of the blasting cycle can be set to the average blasting cycle duration length. For blasting cycles whose actual duration exceeds the average value, only the MS information within the initial period equal to the average duration length is considered and calculated. For blasting cycles with an actual duration shorter than the average value, all MS information of the cycle is included in the subsequent statistics and calculations, and the MS information in the remaining period at the end of the blasting cycle is set to 0.
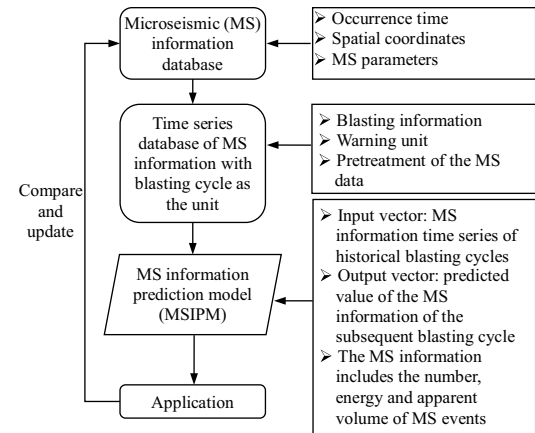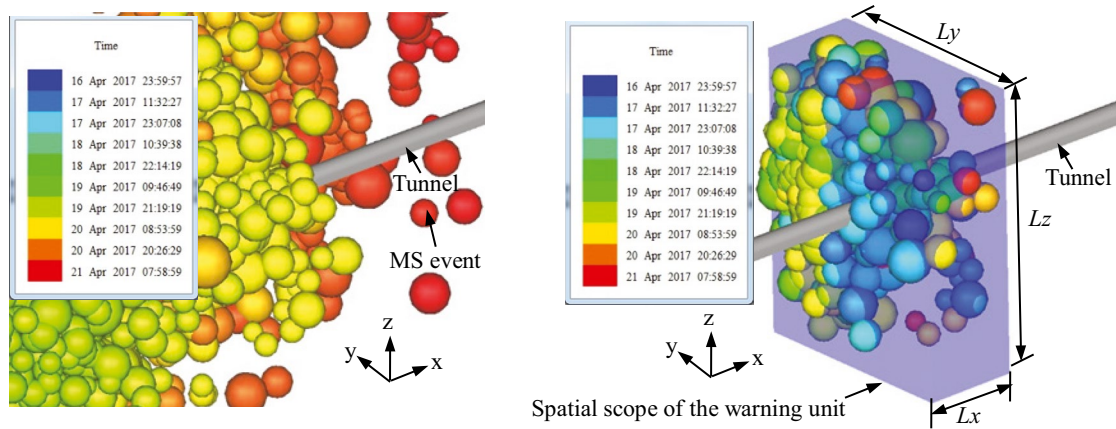
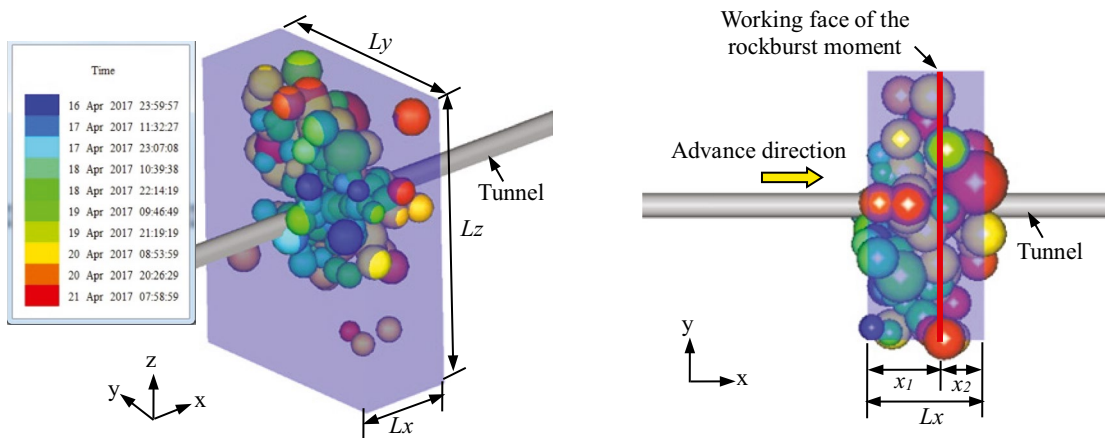**(a)** Establishment of the MS information prediction model
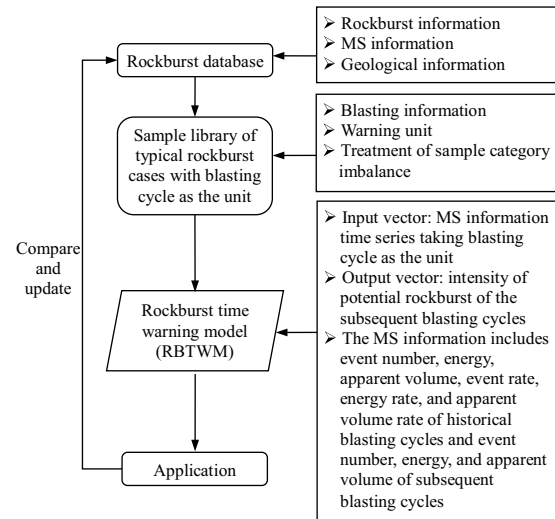
(b) Establishment of the rockburst time warning model
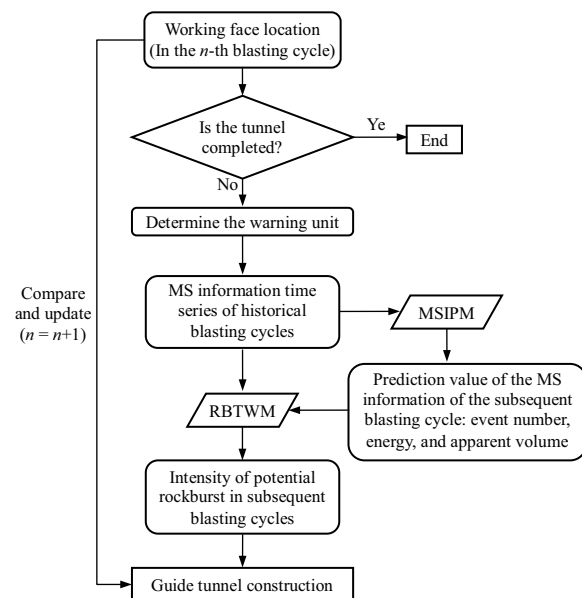
**(c)** Implementation of the warning method

(a) Events are not screened by the warning unit

(b) Events are only screened by the spatial scope of the warning unit

(c) Events are screened by the spatial scope and time span of the warning unit

(d) Top view of (c)

Fig. 3 Spatial scope screening and time span screening effect diagram of rockburst warning unit

Fig. 4 Duration distribution characteristics of each blasting cycle in a tunnel
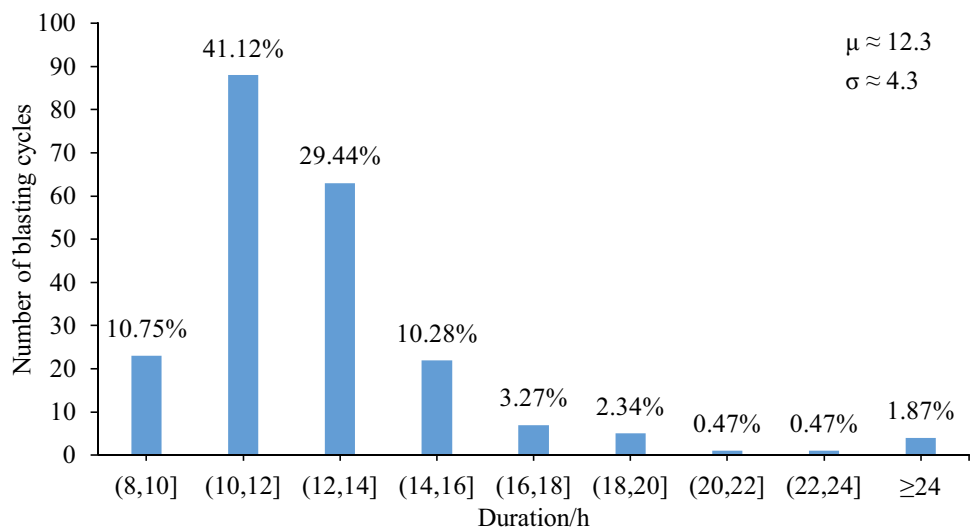
Replacement of missing MS information

Although the MS monitoring system continuously collects MS information over 24 h during tunnel excavation, due to the complex construction site conditions and harsh environments, some blasting cycles inevitably occur during which all or part of the MS monitoring data are lost. For such blasting cycles, the conventional treatment method is to discard them. However, the abandonment of a blasting cycle often results in a discontinuous MS information time series of the adjacent blasting cycles. Therefore, to retain as many samples as possible and fully utilize the acquired MS data, it is necessary to replace any missing data. In this paper, the MSIPM and RBTWM are established to realize the warning of rockburst time taking the blasting cycle as a unit. The MSIPM takes the MS information time series of the historical blasting cycle before the current blasting as input and outputs the MS information of the subsequent blasting cycle. Therefore, the MSIPM can be adopted to fill in any missing data, and the basic steps are as follows:

1. Selecting the MS information time series of blasting cycles with complete data as samples, a generation i MSIPM is trained, and the input vector of this model consists of the MS information time series of n consecutive blasting cycles.
2. For blasting cycles with missing data, it is assessed whether a cycle occurs with missing data among the n cycles before the given cycle, and if so, the cycle is temporarily discarded. Otherwise, the process proceeds to step (3).
3. A time series composed of the MS information of n cycles before the cycle with missing data is input into the generation i MSIPM, the predicted MS information of the given cycle is output after calculation, and the predicted MS information is used to replace the MS information of the given cycle.
4. For blasting cycles with complete data and blasting cycles with replacement MS information obtained in step (3) as samples, a generation $i + 1$ MSIPM is trained, and the input vector of the model is composed of the MS information time series of n consecutive blasting cycles.
5. In regard to blasting cycles with missing data and no replacement information, it is assessed whether a cycle with missing data and no replacement information occurs among the n cycles before the given cycle, and if so, the cycle is temporarily abandoned. Otherwise, the generation i MSIPM is replaced with the generation $i + 1$ MSIPM to perform step (3).
6. Steps (4) and (5) are repeated until replacement values are obtained for all effective blasting cycles with missing data. It should be noted that to control the error intro-

duced by the value replacement process, the above data replacement method is applied only when the number of continuous cycles with missing data does not exceed three, and the case with more than three cycles should be discarded.

Treatment of sample category imbalance

Rockburst warning is a multiclass classification problem, and the warning results include 5 intensities of potential rockburst. Generally, the higher the rockburst intensity is, the smaller its proportion is in all rockburst cases of the same project. This causes the sample category imbalance phenomenon in the rockburst warning method based on deep learning. When the sample category is unbalanced, the algorithm tends to classify high-intensity rockburst as low-intensity rockburst or even no rockburst. However, once rockburst occurs, this may cause numerous casualties and high economic losses, and the higher the rockburst intensity is, the more serious the consequences. Therefore, only by solving the rockburst sample category imbalance problem can we truly improve the rockburst warning accuracy and achieve suitable prevention and control effects.

The most common methods to address the rockburst sample category imbalance problem are undersampling and oversampling. However, in the early stage of tunnel excavation, the number of rockburst cases is slightly insufficient for deep learning purposes; each case is valuable, and there are often only a dozen high-intensity rockbursts. If the undersampling method is adopted to achieve sample balance, many rockburst cases may be lost, thus resulting in the loss of useful information, which adversely impacts the model prediction effect. If the oversampling method (simply copying the minority of samples) is applied to achieve sample balance, this could lead to overfitting of the copied samples, which still leads to a poor model prediction effect.

In summary, for rockburst warnings, to balance the number of rockburst samples of different intensities, a data enhancement method similar to joint under- and oversampling is adopted. In particular, some no rockburst samples (the majority of the samples) are discarded according to certain rules, and virtual moderate or high-intensity rockburst samples (the minority of the samples) are synthesized according to certain rules. Moreover, to improve the reliability of the virtual samples and reduce the negative effects of overfitting, the synthetic minority oversampling technique (SMOTE) (Chawla et al. 2002) is applied instead of simply copying or simulating the existing moderate or high-intensity rockburst samples. The process of realizing the equalization of rockburst samples of different intensities is shown in Fig. 5, and the specific steps are as follows:

1. Through statistical analysis of the distribution characteristics of rockburst samples of different intensities in the original rockburst sample library, the number of rockburst samples for each intensity is obtained, which is recorded as N_N, N_S, N_M, N_I, and N_{EI}.

2. Some no rockburst samples are regularly discarded. First, the no-rockburst samples containing the following two kinds of blasting cycles are discarded: (a) blasting cycles whose actual duration exceeds 2 times the average blasting cycle duration or more; (b) blasting cycles with missing MS monitoring data. Second, some samples are randomly removed from the remaining no rockburst samples so that the number of new no rockburst samples (recorded as N'_N) approaches that of the slight rockburst samples (recorded as N_S).

3. The SMOTE method is applied to moderate and high-intensity rockburst samples. Choosing the moderate rockburst intensity as an example, the core idea of the algorithm is described as follows: (a) for each sample (recorded as x^i_M) in the original moderate rockburst sample set (recorded as S_M), the cluster analysis method is employed to calculate the distance between x^i_M and all other samples in S_M, and the k_M samples closest to x^i_M are identified (recorded as $x^{ijk_M}_M$), where k_M is equal to the sampling rate, namely, $k_M = \langle N_S/N_M \rangle$, and $\langle x \rangle$ indicates that x is rounded; (b) for each x^i_M and $x^{ijk_M}_M$, virtual moderate rockburst samples are synthesized according to the following equation:

$$x^{ij}_{M-new} = x^i_M + rand(0, 1) \bullet \left(x^i_M - x^{ijk_M}_M \right) \tag{2}$$

where x^{ij}_{M-new} is a virtual moderate rockburst sample based on x^i_M and $x^{ijk_M}_M$, and $rand(0, 1)$ is a random number between 0 and 1.

Fig. 5 Flowchart for the realization of the equalization of the rockburst samples of different intensities
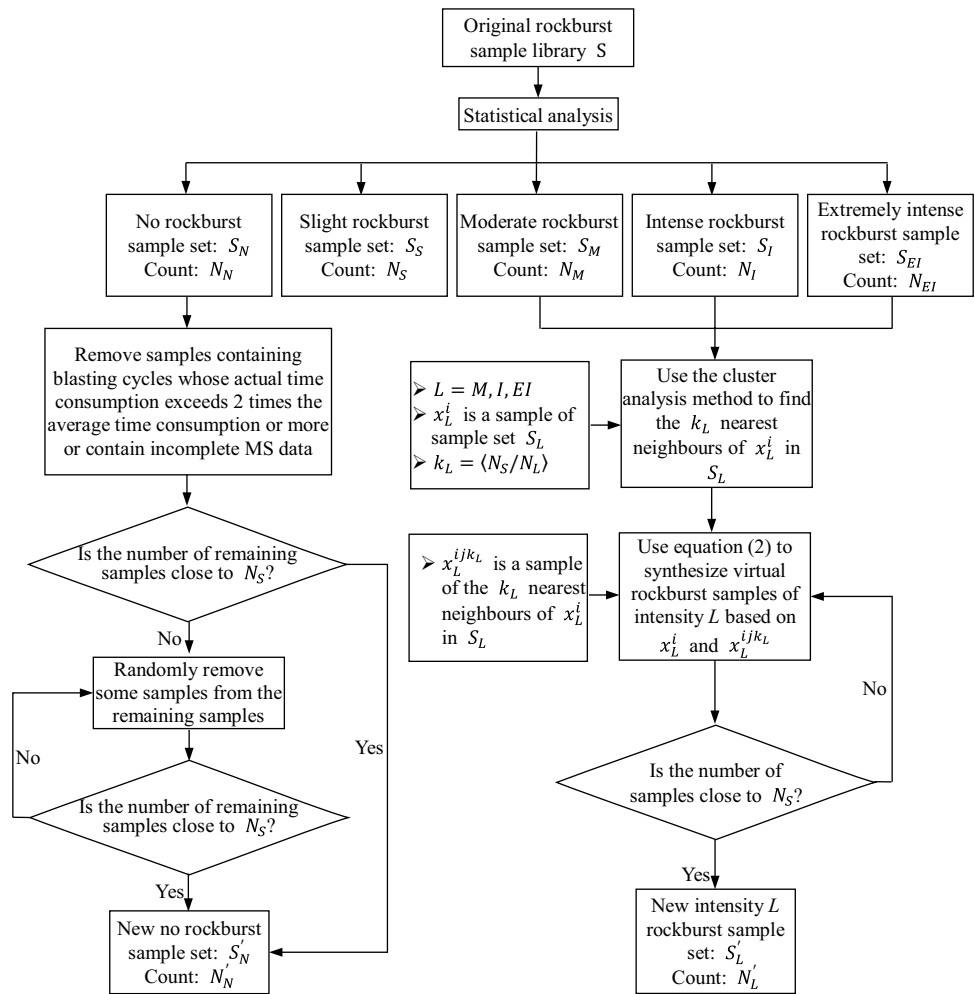
Establishment of the immediate rockburst time warning model

MSIPM

Sample library of the MS information time series

The establishment of a sample library of MS information time series constitutes the basis for MSIPM development. Only a reliable sample library can train an effective prediction model. The main steps to build a sample library are as follows:

1. Extraction of rock mass rupture events and blasting events. The MS data recorded by the MS system contain not only rock mass rupture signals but also various noise signals. Therefore, we need to filter, identify, locate, and analyze these MS data to obtain rock mass rupture events and blasting events and their MS parameters.

2. Selection of the MS parameters. Each MS event contains multiple MS parameters, such as the MS event number, energy, energy index, apparent volume, apparent stress, seismic moment, and stress drop. These MS parameters contain rich rock mass rupture information (Xiao et al. 2016). However, correlations occur among several MS parameters, so it is not necessary to use all MS parameters. Moreover, if all MS parameters are adopted as input data for the subsequent rockburst time warning model, redundancy and noise may occur between the parameters, which decreases the sample separability and prediction accuracy. Therefore, it is necessary to reduce the dimensionality of the MS information and select the most appropriate MS parameters as the target prediction parameters. After years of research, Feng et al. (2015a, b) found that the most basic MS parameters that are reliably independent and reveal the characteristics of microseismicity during the development process of rockburst mainly include the MS event number, energy, and apparent volume. Therefore, this paper selects these three parameters to establish the MSIPM and considers them for the subsequent rockburst warning method.

3. MS information time series samples. The MS information time series samples are arranged in chronological order by the MS information of the historical blasting cycle before the current blasting. The cumulative value of each MS parameter in a given blasting cycle constitutes a component of a sampling point. Each sampling point contains three components, namely, the MS event number, energy and apparent volume, which are represented by $l = 1$, 2, and 3, respectively. One MS information time series sample for the MSIPM is summarized in Table 1. With the excavation of the tunnel, the working face advances, and the warning unit also moves forward. Therefore, new MS information time series samples are added every time a new blasting cycle is implemented.

The network structure of the MSIPM

The MSIPM based on LSTM is mainly composed of an input layer, hidden layer, and output layer. A dropout layer is also introduced to prevent the model from overfitting during training. The structure is shown in Fig. 6a. The input vector includes the MS information time series samples before the current blasting cycle, and the output vector includes the MS information of the next blasting cycle. The relational expression is:

$$m_l^{t+i} = \Phi\left(m_l^n, m_l^{n-1}, \cdots, m_l^3, m_l^2, m_l^1\right) \tag{3}$$

where m_l^{t+i} is the predicted value of MS information l of the i-th blasting cycle after the current blasting cycle for $i = 1$, 2, 3, m_l^n is the value of MS information l of the n-th blasting cycle before the current blasting cycle, and Φ is the nonlinear relationship between the MS information of the subsequent blasting cycle and the MS information time series of the historical blasting cycle before the current blasting.

Training and testing of the MSIPM

Only through training and testing can the MSIPM learn the deep features of MS information evolution with the blasting cycle and predict the future development trend of the MS information according to the historical input data. After the MS information time series sample database is established, the first 70% of the samples in the sample database are selected as training samples, and the remaining 30% of the samples are adopted as test samples to train and test the

Table 1 One MS information time series sample for the MS information prediction model

MS parameters \ Number of the blasting cycle	322	323	324	325	326	327	328	329
MS event number	7	17	14	8	16	17	27	6
MS energy/10^3J	1.072	2.0751	5.5089	3.9322	12.435	12.559	10.419	13.238
MS apparent volume/10^3m^3	2.2247	13.935	8.5095	4.1328	3.6291	2.9405	11.566	1.3399

(a) MS information prediction model

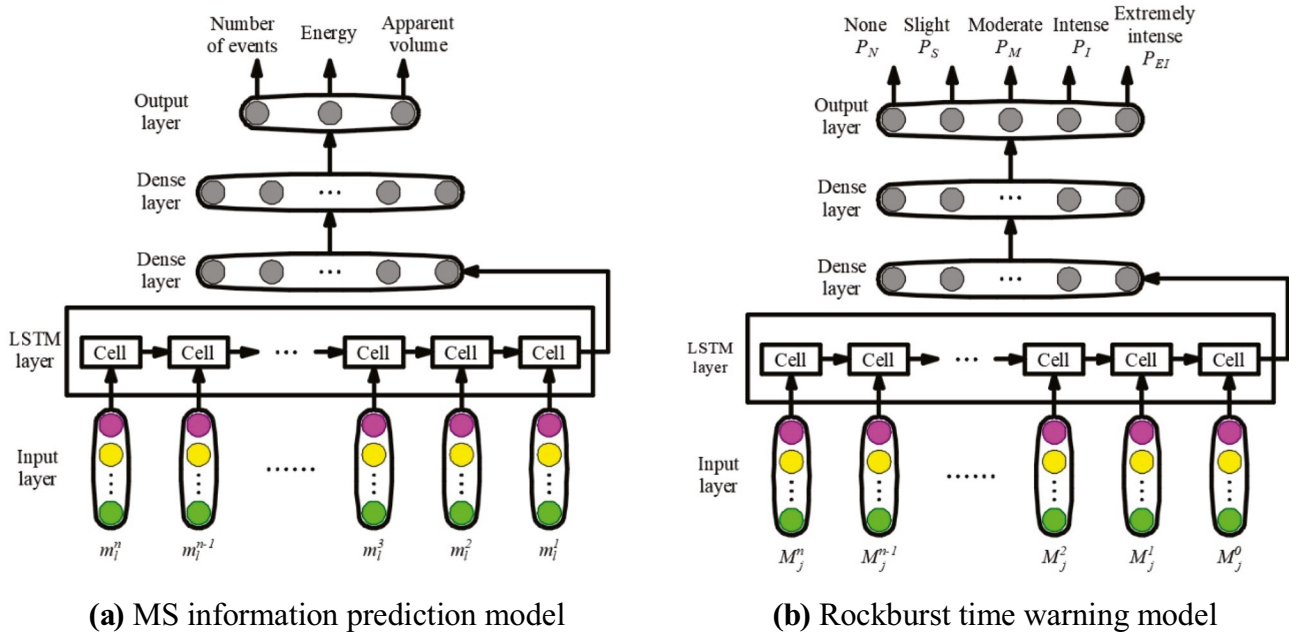**(b)** Rockburst time warning model

Fig. 6 Basic structure of the MS information prediction model and rockburst time warning model based on LSTM

model. As the predicted value is the MS information of the subsequent blasting cycle, which is a concrete numerical value, the root mean square error (RMSE) is applied as the loss function, and its expression is as follows:

$$RMSE = \sqrt{\frac{1}{n}\sum_{i=1}^{n}\left(y_i - y_i'\right)^2} \tag{4}$$

where y_i is the original value of the i-th data in a batch of data, y_i' is the predicted value of y_i given by the LSTM, and n is the number of batches of data.

The coefficient of determination (R^2) is adopted to measure the prediction accuracy of the model. The calculation equation for the coefficient of determination is as follows:

$$R^2 = 1 - \frac{\sum_{i=1}^{n}\left(y_i - y_i'\right)^2}{\sum_{i=1}^{n}\left(y_i - \bar{y}\right)^2} \tag{5}$$

where $\bar{y}$ is the average value of the original data, and the closer R^2 is to 1, the higher the prediction accuracy of the model.

The MSIPM based on the LSTM is obtained after training. The samples in the test set are input into the MSIPM, and the predicted value of the target vector is obtained through calculation. The RMSE of the test set is then calculated based on the predicted and original values. The performance of the MSIPM is measured through the RMSE. The model is optimized by adjusting the network parameters of

the LSTM when the MSIPM performance does not satisfy the requirements. The adjustable parameters mainly include the number of hidden layers (n_hidden_layer), node number of hidden layers (n_hidden_node), time step size (step_size), number of data points processed in a batch (batch_size), probability of the dropout layer, and maximum number of times to traverse all samples in the training set (epoch).

RBTWM

The core idea of the RBTWM is that by taking the actual rockburst situations and MS information of each blasting cycle as samples, the deep learning method is applied to mine and characterize the deep features between them to realize the warning method of the immediate rockburst time in blasting cycle units. The establishment process of the RBTWM is similar to that of the MSIPM, mainly including the establishment of a rockburst database, the establishment of a corresponding MS information time series database, the treatment of sample category imbalance, the selection of MS parameters, and the training, testing, optimization, and dynamic updating of the model.

The rockburst database is largely established according to the actual rockburst situations of each blasting cycle on site. It is necessary to record information such as the location, time, type, and intensity of the rockburst, and the excavation and support conditions. The input vector of the RBTWM includes the MS information time series obtained by fusing MS information from historical and subsequent blasting cycles. The output vector of the RBTWM includes

the potential rockburst intensity and during which blasting cycle it may occur. The components of each sampling point of the input vector include the cumulative MS event number, cumulative MS energy, cumulative MS apparent volume, MS event rate, MS energy rate, and MS apparent volume rate of the historical blasting cycle before the current blasting cycle and the MS event number, MS energy, and MS apparent volume of the subsequent blasting cycles, which are expressed as $j = 1, 2, 3, …$, where $j = 1$ to 6 indicate the first six parameters, while $j = 7$ to 9 indicate the MS event number, MS energy, and MS apparent volume of the first subsequent blasting cycle. Moreover, $j = 10$ to 12 indicates the 3 parameters of the second subsequent blasting cycle, and $j = 13$ to 15 indicate the 3 parameters of the third subsequent blasting cycle. When the maximum value of j is 9, 12, or 15, the RBTWM can output the potential rockburst intensity of the first, second, and third subsequent blasting cycles, respectively. One MS information time series sample for the RBTWM is listed in Table 2. With the excavation of the tunnel, the working face continuously moves forward, and the warning unit also moves forward. Therefore, a new sample is added every time a new blasting cycle is implemented.

The network structure of the RBTWM based on LSTM is similar to that of the MSIPM, and it is also primarily composed of an input layer, hidden layer, output layer, and dropout layer. Its structure is shown in Fig. 6b. The relationship between the input and output vectors is as follows:

$$P_d = f\left(M_j^n, M_j^{n-1}, \cdots, M_j^3, M_j^2, M_j^1 \right) \tag{6}$$

where P_d indicates the probability that a rockburst of intensity d may occur in the subsequent blasting cycle, d is the rockburst intensity, including no, slight, moderate, intense, and extremely intense rockburst, f is the nonlinear relationship between the rockburst intensity and MS information, and M_j^n is the value of MS information j in the warning unit of the n-th blasting cycle before the current blasting cycle. With respect to the MS information for which the true value has not been obtained when a warning is issued, the predicted value calculated by the MSIPM is considered instead, for example,

$$\begin{pmatrix} M_7^1 & M_8^1 & M_9^1 \\ M_{10}^1 & M_{11}^1 & M_{12}^1 \\ M_{13}^1 & M_{14}^1 & M_{15}^1 \end{pmatrix} = \begin{pmatrix} m_1^{t+1} & m_2^{t+1} & m_3^{t+1} \\ m_1^{t+2} & m_2^{t+2} & m_3^{t+2} \\ m_1^{t+3} & m_2^{t+3} & m_3^{t+3} \end{pmatrix} \tag{7}$$

The meaning of m_l^{t+i} is the same as in Eq. (3).

Equations (6) and (7) indicate that the RBTWM comprehensively considers the cumulative value of the MS parameters of the historical blasting cycle before the current blasting cycle, the average daily change rate, and the value of the MS parameters of the subsequent blasting cycles. The multiparameter warning may avoid the one-sidedness and limitation of the single-factor warning.

Table 2 One MS information time series sample for the rockburst time warning model

MS parameters \ Number of the blasting cycle	322	323	324	325	326	327	328	329
Cumulative MS event number	87	76	79	79	78	86	104	103
Cumulative MS energy/10^3J	13.9610	12.4980	16.4960	18.4420	28.2780	39.4540	47.9830	60.0030
Cumulative MS apparent volume/10^3m^3	72.4850	56.6000	56.1340	54.1860	43.0980	33.8930	42.7950	42.9070
MS event rate/(Pieces/d)	19.3151	16.2704	18.3948	16.7856	15.2278	18.6186	21.7759	19.7449
MS energy rate/(10^3J/d)	3.0995	2.6756	3.8410	3.9185	5.5207	8.5416	10.0468	11.5025
MS apparent volume rate/(10^3 m^3/d)	16.0926	12.1172	13.0706	11.5132	8.4139	7.3377	8.9606	8.2252
MS event number in the first subsequent blasting cycle	17	14	8	16	17	27	6	12
MS energy in the first subsequent blasting cycle/10^3J	2.0751	5.5089	3.9322	12.4350	12.5590	10.4190	13.2380	38.7945
MS apparent volume in the first subsequent blasting cycle/10^3m^3	13.9350	8.5095	4.1328	3.6291	2.9405	11.5660	1.3399	7.226
MS event number in the second subsequent blasting cycle	14	8	16	17	27	6	12	3
MS energy in the second subsequent blasting cycle/10^3J	5.5089	3.9322	12.4350	12.5590	10.4190	13.2380	38.7945	1.2258
MS apparent volume in the second subsequent blasting cycle/10^3 m^3	8.5095	4.1328	3.6291	2.9405	11.5660	1.3399	7.226	7.1619
MS event number in the third subsequent blasting cycle	8	16	17	27	6	12	3	2
MS energy in the third subsequent blasting cycle/10^3J	3.9322	12.4350	12.5590	10.4190	13.2380	38.7945	1.2258	2.0161
MS apparent volume in the third subsequent blasting cycle/10^3 m^3	4.1328	3.6291	2.9405	11.5660	1.3399	7.226	7.1619	5.8811

Considering the MS information of the subsequent blasting cycles improves the accuracy of the rockburst time warning method when taking the blasting cycle as a unit. It should be noted that the relationship between the various MS parameters and potential rockburst intensity is different. In the traditional multiparameter regression analysis method, it is often necessary to apply the search method to assign different weights to the various parameters. However, because this method uses a deep learning algorithm, the weights of each parameter no longer need to be artificially determined but are synchronously obtained during the model training process. The training, testing, optimization, and dynamic update processes of the RBTWM are similar to those of the MSIPM, and they are not described again here.

Implementation of the warning method of the immediate rockburst time

With the establishment of the MSIPM and RBTWM, the intensity of potential rockburst in the subsequent blasting cycles during tunnel excavation can be forecasted. In tunnel engineering, immediate rockburst mainly occurs near the working face, i.e., the area enclosed by the warning unit. In the process of warning implementation, the warning unit should maintain the spatial scope unchanged and advance as a whole following the working face. Before the next blasting cycle starts, first, the spatial coordinates of the warning unit are determined according to the chainage of the working face. Second, the MS information time series of the historical blasting cycle before the current blasting in the spatial scope of the warning unit is input into the MSIPM, and the MS information prediction value of the subsequent blasting cycle is calculated. The original and predicted MS information values are then fused to form an MS information time series, which is then entered into the RBTWM to calculate the intensity of potential rockburst in the subsequent blasting cycle. Therefore, the warning of the immediate rockburst time taking the blasting cycle as the unit is realized.

With an increasing number of blasting cycles, the chainage of the working face, spatial coordinates of the warning unit, and MS information of the warning unit constantly change. Therefore, it is necessary to input the updated MS information into the MSIPM and RBTWM over time to update the warning area and warning results in a timely manner. The corresponding rockburst prevention and control measures should also be adjusted in time.

With the excavation of the tunnel, MS information time series samples and rockburst cases become increasingly abundant. According to the comparison and analysis of the MS information prediction results and rockburst warning results with respect to the actual on-site situations, the MS information time series samples and rockburst databases can be regularly supplemented and updated, and the MSIPM and RBTWM can then be retrained and updated to improve the rockburst warning effect.

The abovementioned warning method of the immediate rockburst time fully utilizes the excellent performance of LSTM in resolving time series problems. The MS information contained in the input vector of the rockburst warning model is not solely acquired by simple cumulative summation; some of the MS information is determined by learning the evolution characteristics of the MS information time series of the historical blasting cycle. Moreover, the input vector not only contains the MS information of a certain blasting cycle but also contains the MS information of several historical blasting cycles arranged in a time sequence. In addition, the MS information screened by the warning unit represents the spatial evolution of MS information in the process of tunnel excavation because the warning unit advances with the working face. Therefore, the MS information contained in the input vector of the rockburst warning model comprehensively reflects the temporal and spatial evolution characteristics of MS information in the rockburst development process, which is of great significance for the improvement of the rockburst time warning effect. Next, the above is further analyzed and verified from the perspective of engineering applications.

Engineering application

Establishment of the MSIPM and RBTWM for the railway tunnel

In the early stage of monitoring of the tunnel, an important task is to accumulate construction information, MS monitoring information, and rockburst cases. With the excavation of the tunnel, the database was updated and supplemented over time. After a certain period of in situ monitoring, the MS information of 245 blasting cycles and the corresponding rockburst cases was collected.

Based on the shape and size of the tunnel cross-section, the equivalent diameter of the tunnel is calculated as 6.6 m. According to the analysis and Eq. (1), it is determined that the spatial scope of the warning unit along the tunnel axis ranges from approximately 25 m behind the working face to 10 m in front of the working face, and along the radial direction of the tunnel, the spatial scope extends approximately 35 m from the tunnel center axis, as shown in Fig. 7.

The MS information of each blasting cycle is extracted after the spatial scope of the warning unit is determined, and the duration of each blasting cycle is then standardized to a uniform length. Any missing data from blasting cycles are replaced by using the blasting cycle processing method described in "Treatment of the blasting cycle." According
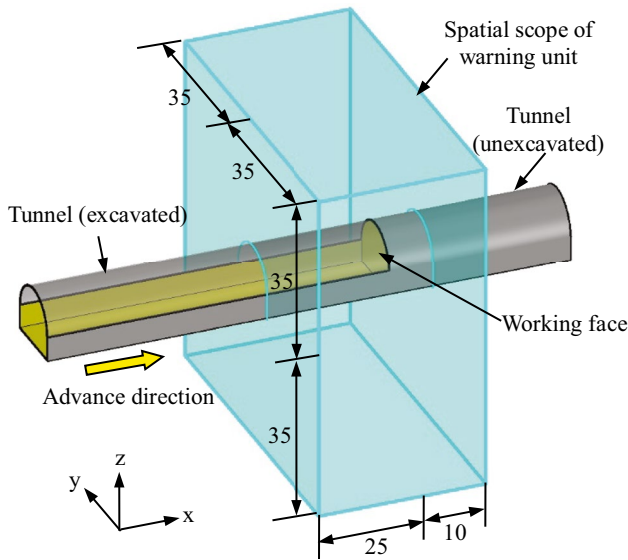
Fig. 7 Spatial scope of the warning unit used for the warning method of the immediate rockburst time in a railway tunnel (unit: m)

to statistical analysis, the length of the blasting cycle after standardization was 12 h, and 225 blasting cycles meeting the above requirements were obtained after filling. There were 20 cycles that did not meet the requirements, mainly because there were more than 3 consecutive cycles in which MS data were not collected, the collected MS data were incomplete, or the duration of these cycles was more than 36 h. Moreover, the actual rockburst situations corresponding to the 225 blasting cycles were determined, and the initial rockburst database was then established.

To train and test the MSIPM and RBTWM, the first 70% of the cases in the MS information database and rockburst database were selected as training samples, and the remaining 30% of the cases were applied as test samples. Figure 8 shows the distribution characteristics of the rockburst cases
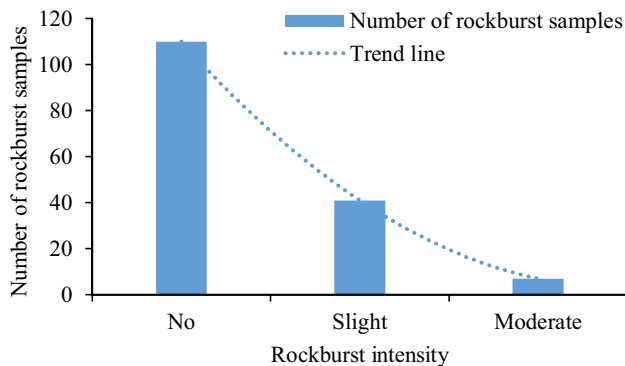
Fig. 8 Distribution characteristics of the rockburst samples of different intensities in the original training sample set

of different intensities in the training samples. The training samples only include no rockburst, slight rockburst, and moderate rockburst samples, and the moderate rockburst samples constitute the minority of the samples, while the no rockburst samples constitute the majority of the samples. There is a large difference between the numbers of minority- and majority-type samples. To resolve the sample category imbalance problem, for the training samples, the corresponding solution described in "Treatment of sample category imbalance" is applied to discard low-quality no-rockburst samples while synthesizing virtual moderate rockburst samples. The processed rockburst database contains 45 no-rockburst samples, 41 slight rockburst samples, and 42 moderate rockburst samples.

Establishment of the MSIPM

The structure of the MSIPM is shown in Fig. 6a. The final network structure obtained through training and testing includes (1) an input layer, used to input the MS information time series samples before the current blasting, (2) a hidden layer, including 64 LSTM cells, (3) a dropout layer, with a probability of 0.1, and (4) an output layer, including three nodes corresponding to the number of MS parameters to be predicted (the MS event number, energy, and apparent volume of the next blasting cycle). In addition, step_size is set to 8: namely, the MS information of the next blasting cycle is predicted by the MS information of 8 historical blasting cycles before the current blasting cycle. The batch_size variable is set to 12, and the epoch variable is set to 500.

After obtaining the MSIPM, the test samples are input into the MSIPM following the method described in "Training and testing of the MSIPM," and the predicted values of the test sets are calculated. Then, by integrating the predicted values of the first subsequent cycle of each sample in the test set into the input vector, the predicted values of the second subsequent cycle of each sample are obtained, and the predicted values of the third subsequent cycle are determined with the same method. Therefore, the predicted value of each sample in the test set includes the predicted value of the MS information of the three subsequent blasting cycles. For convenience, the blasting cycle of the first sample in the test set is recorded as the first blasting cycle. The comparative analysis results of the predicted values of the test set and the original data are shown in Fig. 9.

Figure 9 reveals that the variation trends of the predicted values of the MS event number, energy, and apparent volume of the test set are essentially consistent with those of the original data. In regard to the blasting cycle with a sudden increase in the original MS information, the predicted value is smaller than the original data as a whole. The evolution of the error and the coefficient of determination of the MS information prediction value in
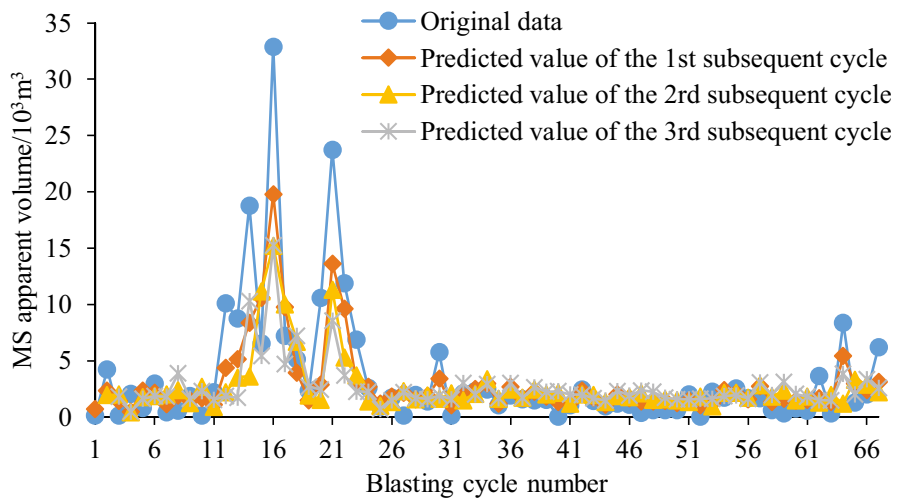
Fig. 9 Comparative analysis results between the predicted values of the MS parameters and the original data in the test set
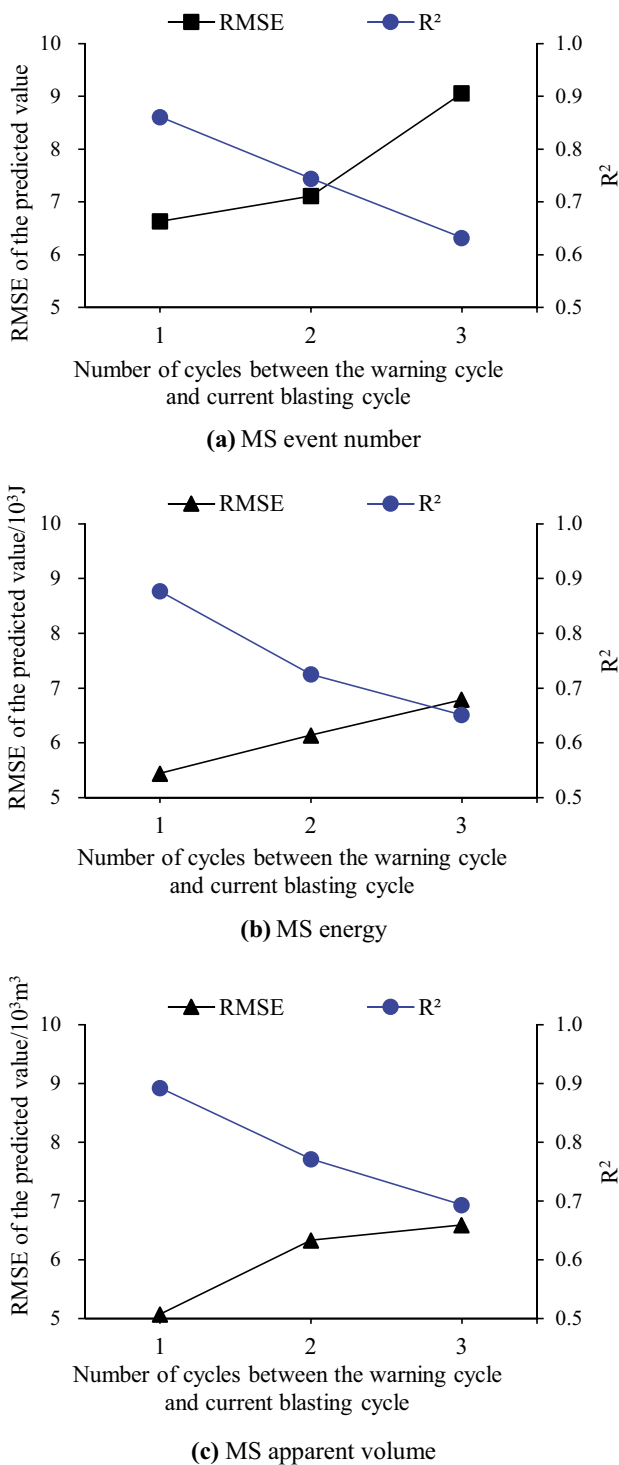

(a) MS event number

(b) MS energy

(c) MS apparent volume
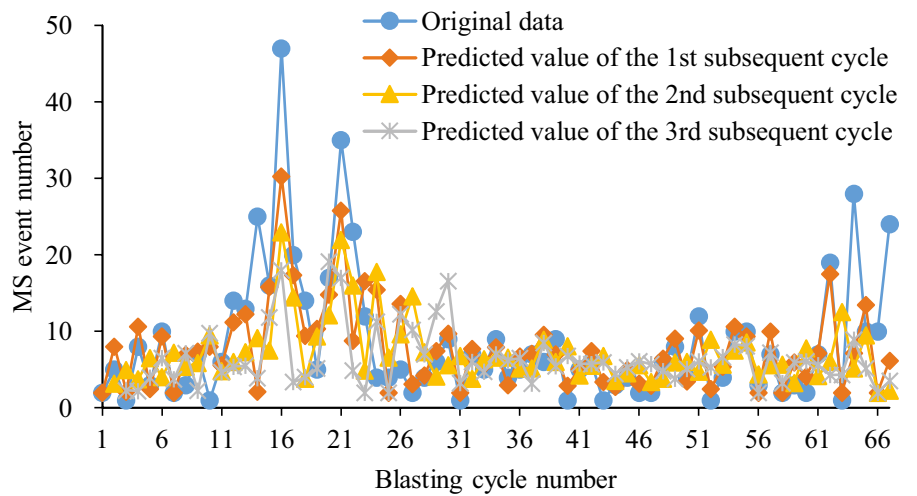
(a) MS event number
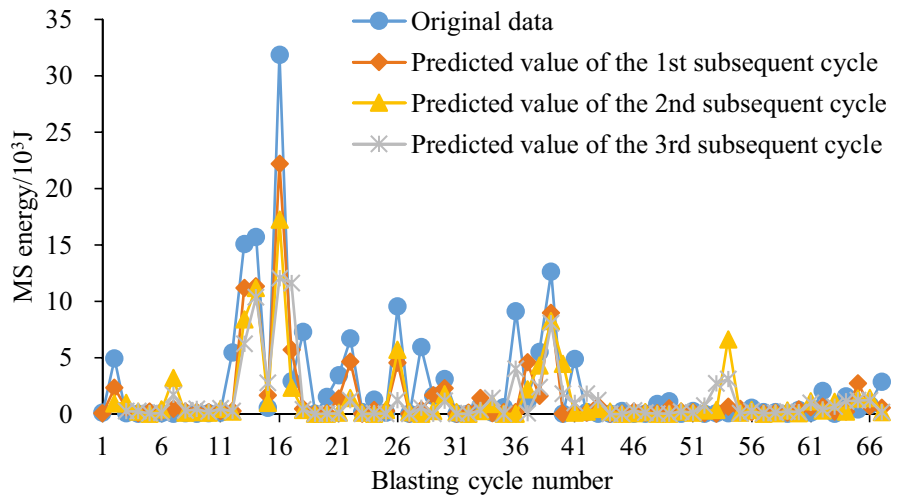
(b) MS energy

(c) MS apparent volume

Fig. 10 Evolution of the RMSE and R^2 of the predicted values of the MS parameters with the interval between the predicted and current blasting cycles

the subsequent blasting cycle with the interval between the predicted and current blasting cycles are shown in Fig. 10. It is evident from Fig. 10 that larger intervals between the predicted and current blasting cycles correlate with larger

errors in the MS information prediction value and smaller coefficients of determination.

Establishment of the RBTWM

The structure of the RBTWM is shown in Fig. 6b. The final network structure obtained through training and testing includes (1) an input layer, used to input the MS information time series obtained by fusing MS information from historical and subsequent blasting cycles, (2) a hidden layer, including 112 LSTM cells, (3) a dropout layer, with a probability of 0.1, and (4) an output layer, including three nodes corresponding to the classification number of the rockburst intensities to be considered in the rockburst warning method (when this model was established, only no rockburst, slight rockburst, and moderate rockburst occurred in the tunnel; higher-intensity rockburst samples will be supplemented, and the model will be updated in the future). The softmax function is adopted to output the potential rockburst intensity of the subsequent blasting cycles. In addition, step_size is set to 8, namely, the intensity of potential rockburst in the subsequent blasting cycles is predicted by the MS information time series of 8 historical blasting cycles. The batch_size variable is set to 12, and the number of epochs is set to 500.

The MS information of the historical and subsequent blasting cycles corresponding to each sample in the test set are fused to form the input vector of the RBTWM. The method described in "RBTWM" is then applied to input the vector into the RBTWM, and the warning results of the test set are calculated. Every time the warning results are released, the intensity values of potential rockbursts of the three subsequent blasting cycles after the current blasting cycle are given. The warning results of the test set and the actual rockburst situations on site are shown in Fig. 11.

On the basis of Fig. 11, the warning results of the 1st, 2nd, and 3rd subsequent blasting cycles are compared and analyzed to the actual rockburst situations on site, and the confusion matrix is obtained, as shown in Fig. 12. To further analyze the warning effect of the abovementioned RBTWM, it is necessary to statistically analyze the warning accuracy of each blasting cycle. In this paper, the warning accuracy of each blasting cycle was determined according to a relatively strict calculation method: namely, when the rockburst intensity of a blasting cycle predicted by the RBTWM is the same as the actual rockburst intensity on site, the warning is regarded as accurate. Otherwise, it is regarded as inaccurate. Every time warning results are issued, a warning is given in regard to the three cycles after the current blasting, and the warning accuracies of the three subsequent cycles are calculated. The calculation equation for the warning accuracy is as follows:

Fig. 11 Warning results of the test set calculated by the RBTWM and actual rockburst intensity

(a) 1-10 blasting cycles

(b) 11-21 blasting cycles

(c) 22-32 blasting cycles

(d) 33-43 blasting cycles

Fig. 11 (continued)

Number of blasting cycle	45	46	47	48	49	50	51	52	53	54	55	56	57
Actual rockburst intensity													
Warning results and release time (during the i-th blasting cycle) 44													
45													
46													
47													
48													
49													
50													
51													
52													
53													
54													

(e) 44-54 blasting cycles

Number of blasting cycle	56	57	58	59	60	61	62	63	64	65	66	67	
Actual rockburst intensity													
Warning results and release time (during the i-th blasting cycle) 55													
56													
57													
58													
59													
60													
61													
62													
63													
64													
65													
66													

(f) 55-66 blasting cycles

$$A_i = \frac{T_i^t}{T_i} \tag{8}$$

where A_i is the warning accuracy of the i-th blasting cycle after the current blasting for $i = 1, 2, 3$, T_i^t is the number of times that the warning rockburst intensity of the i-th blasting cycle after the current blasting is the same as the actual rockburst intensity on site, and T_i is the number of warnings for the i-th blasting cycle after the current blasting. In addition, the recall rate (Bi et al. 2022) is used to evaluate the warning performance of the model for different intensities of rockburst in different subsequent blasting cycles. The higher the recall rate, the better the warning performance of the model.

According to the confusion matrix shown in Fig. 12, based on the test set, the rockburst warning accuracies for the 1st, 2nd, and 3rd subsequent blasting cycles are approximately 74.6% (50/67), 71.2% (47/66), and 63.1% (41/65), respectively. Figure 13 shows the evolution of the rockburst warning accuracy of the subsequent blasting cycles with the interval between the warning and current cycles. Figure 13 reveals that the larger the interval between the warning and current blasting cycles is, the lower the rockburst warning accuracy becomes. Therefore, the timing of a potential rockburst in the subsequent blasting cycle should be based on the latest rockburst warning result. Figure 14 shows the recall rate distribution characteristics of warning of different intensities of rockbursts in different subsequent blasting cycles. Figure 14 reveals that the model has the best warning performance for moderate rockburst, followed by no rockburst. It also reveals that the larger the interval between the warning and current blasting cycles is, the worse the warning performance.

Implementation of the rockburst time warning method in the railway tunnel

After the MSIPM and RBTWM are established, the immediate rockburst time warning method, taking the blasting cycle as the unit, is implemented during tunnel construction. The following selects the tunnel excavation from September 18, 2018, to September 24, 2018, from chainage DK196+528 to chainage DK196+558, as an example to describe the implementation process of the warning method of the immediate rockburst time in detail.

### Warning of the immediate rockburst time taking the blasting cycle as the unit

At 20:00 on September 18, 2018, the tunnel was ready for blasting, and the chainage of the working face before blasting was DK196+528. For convenience, this blasting cycle is recorded as the 330th blasting cycle. The MS information
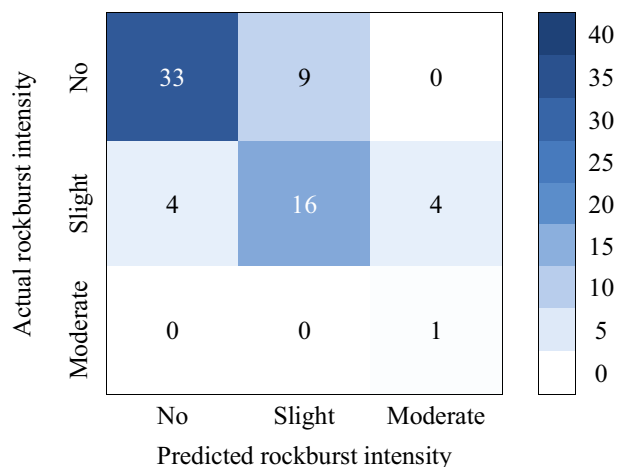
(a) The first subsequent blasting cycle
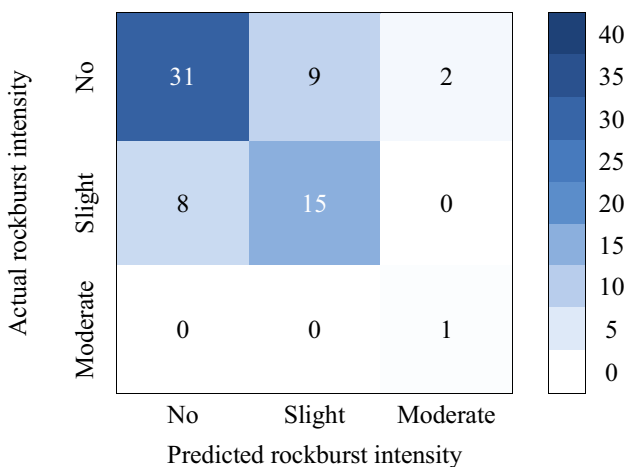
(b) The second subsequent blasting cycle
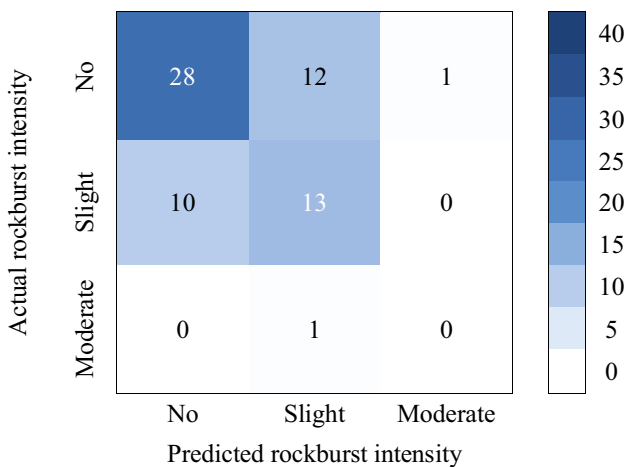
(c) The third subsequent blasting cycle

Fig. 12 Confusion matrix of the comparison of the warning results of the test set calculated by the RBTWM and actual rockburst intensity
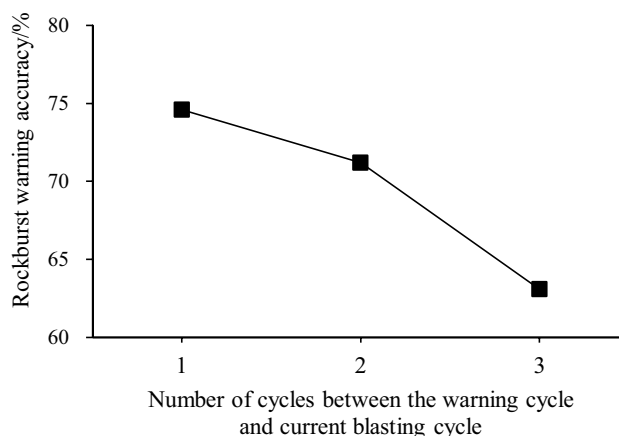

Fig. 13 Evolution of the rockburst warning accuracy with the interval between the warning and current blasting cycles

time series of the historical blasting cycle before the current blasting is provided in Table 1. The data were entered into the MSIPM established in "Establishment of the MSIPM," and the predicted values of the MS information of the subsequent three blasting cycles obtained are summarized in Table 3. The MS information contained in Tables 1 and 3 was fused to obtain the MS information time series for rockburst warning purposes for the subsequent blasting cycle, as indicated in Table 2. The information was input into the RBTWM established in "Establishment of the RBTWM," and warning results for the potential rockbursts of the three subsequent blasting cycles (i.e., the 330th, 331st, and 332nd blasting cycles) were obtained, as shown in Fig. 15. By repeating the above steps before the start of each blasting cycle, the corresponding warning results of the potential immediate rockburst of the subsequent blasting cycles were determined. As shown in Fig. 16, from September 18, 2018, to September 24, 2018, rockburst warnings were issued for 10 blasting cycles in the tunnel.
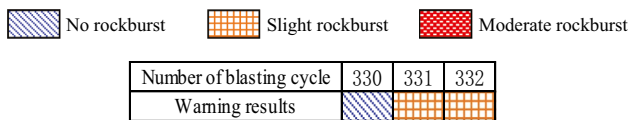
Actual situation on site

Site survey photographs near the working faces of the 10 blasting cycles are shown in Fig. 17. In these 10 blasting cycles, 2 slight and 2 moderate rockbursts occurred. Among them, the first moderate rockburst occurred at 11:30 on September 21, 2018 (during the 335th blasting cycle), and the rockburst pit was funnel-shaped with a size of 2 m × 2 m × 0.5 m (length × width × depth), as shown in Fig. 17f. The second moderate rockburst occurred at 9:30 on September 23, 2018 (during the 338th blasting cycle), and the rockburst pit was also funnel-shaped with a size of 2 m × 2 m × 0.5 m, as shown in Fig. 17i. Figure 16 also shows that the blasting cycles during which the two moderate rockbursts occurred are all successfully warned, and warnings are issued two

Fig. 14 Recall rate distribution characteristics of warning of different intensity rockbursts in different subsequent blasting cycles
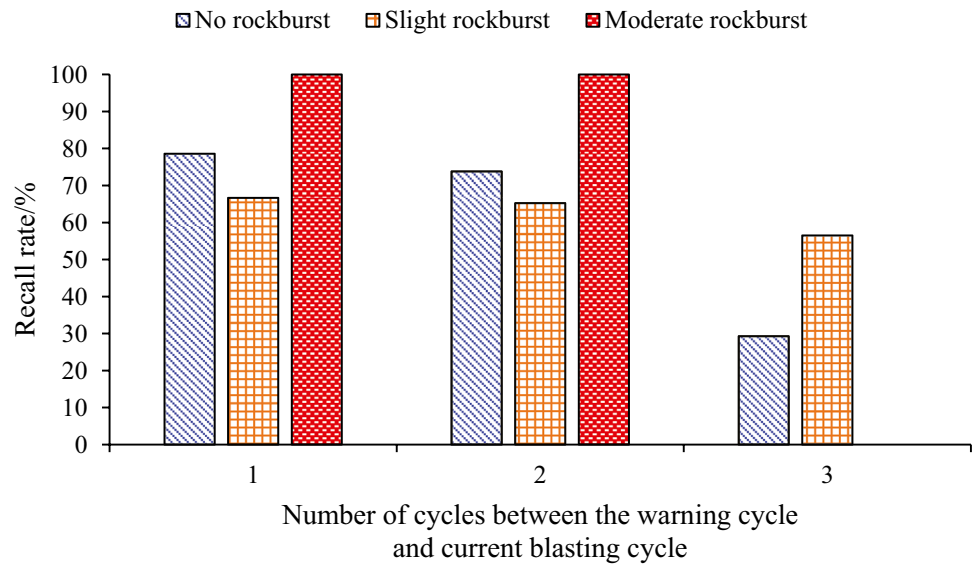
Table 3 Prediction value of the MS information of the subsequent blasting cycle after the 329th blasting cycle

MS parameters \ Number of the blasting cycle	330	331	332
MS event number	12	3	2
MS energy/10^3J	38.7945	1.2258	2.0161
MS apparent volume/10^3m^3	7.2260	7.1619	5.8811

□ No rockburst   □ Slight rockburst   ▣ Moderate rockburst

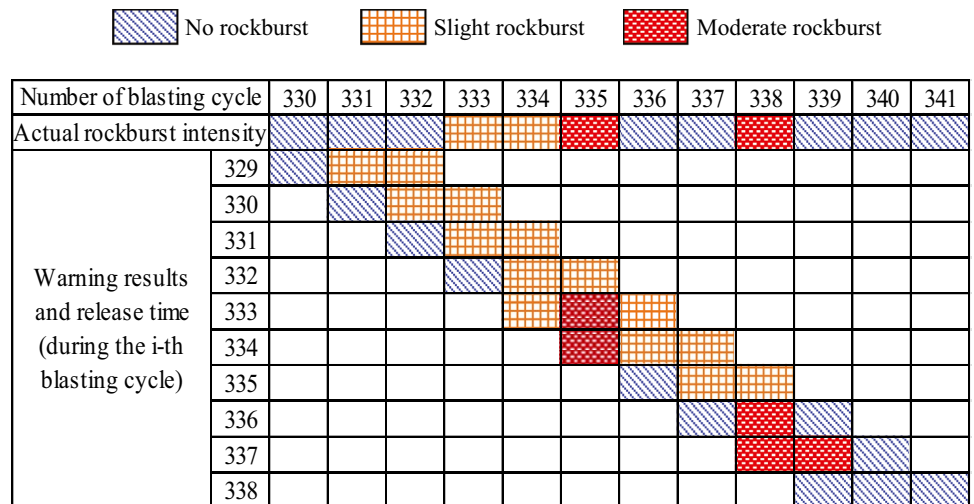| Number of blasting cycle	330	331	332
Warning results	No rockburst	Slight rockburst	Slight rockburst

Fig. 15 Warning results of the potential immediate rockburst in the subsequent blasting cycle after the 330th blasting cycle

blasting cycles ahead. It is also evident from Fig. 16 that if only the warning results of the first subsequent cycle are
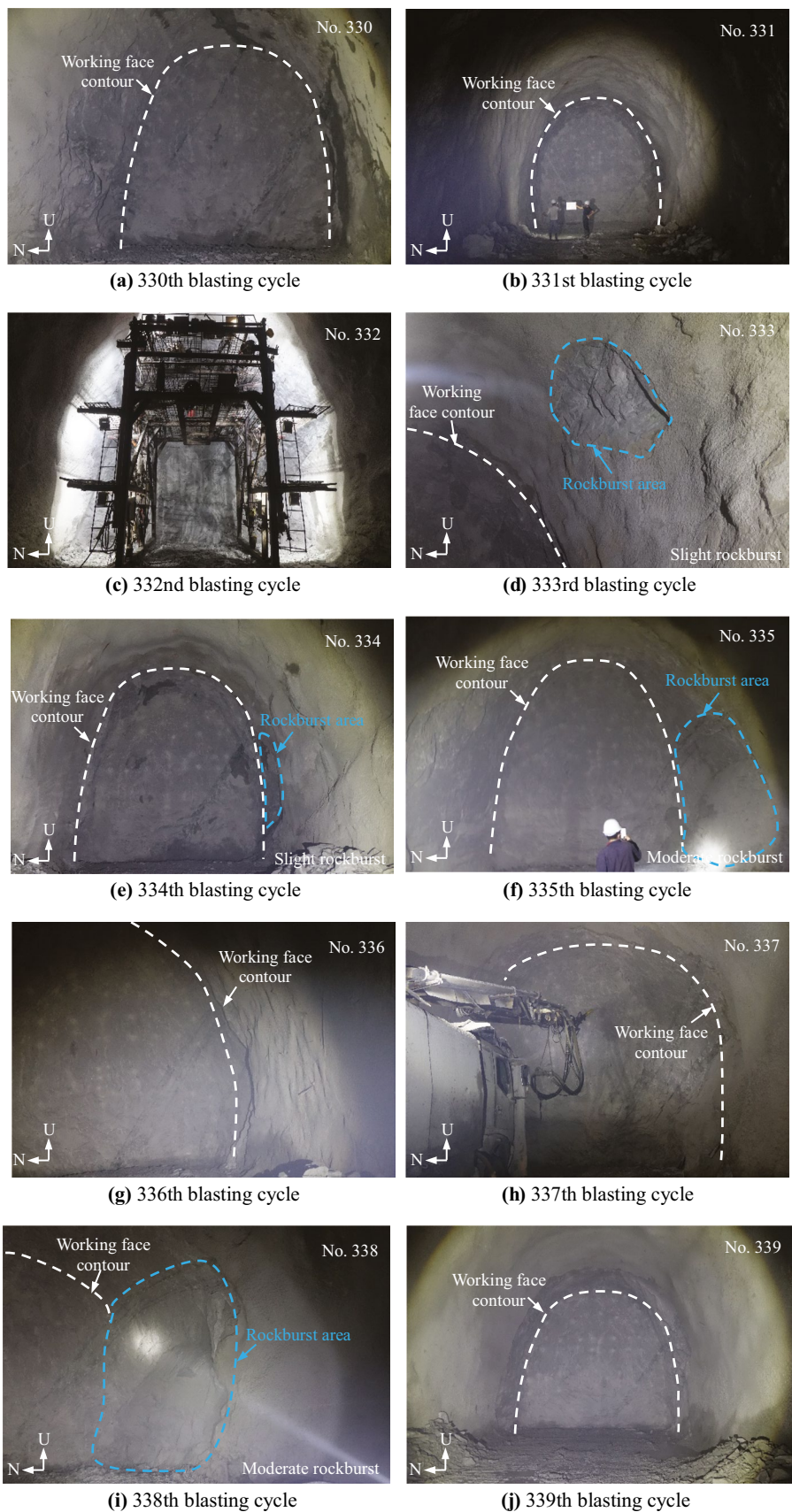
considered, warning only successfully results for one of the two blasting cycles during which the two slight rockbursts occurred. If the warning results of the first and second subsequent cycles are combined, warning successfully results for both blasting cycles during which the two slight rockbursts occurred. Because the warning of potential rockbursts was issued before the start of the related blasting cycles and the on-site construction personnel implemented corresponding prevention and control measures, the above four rockbursts did not cause any casualties or equipment losses.

Fig. 16 Rockburst warning results of each blasting cycle from September 18, 2018, to September 24, 2018, and the actual rockburst conditions on site

□ No rockburst   □ Slight rockburst   ▣ Moderate rockburst

Number of blasting cycle		330	331	332	333	334	335	336	337	338	339	340	341
Actual rockburst intensity		No rockburst	No rockburst	No rockburst	Slight	Slight	Moderate	No rockburst	No rockburst	Moderate	No rockburst	No rockburst	No rockburst
Warning results and release time (during the i-th blasting cycle)	329	No rockburst	Slight	Slight									
	330		No rockburst	Slight	Slight								
	331			No rockburst	Slight	Slight							
	332				No rockburst	Slight	Slight						
	333					Slight	Moderate	Slight					
	334						Moderate	Slight	Slight				
	335							No rockburst	Slight	Slight			
	336								No rockburst	Moderate	No rockburst		
	337									Moderate	No rockburst		
	338										No rockburst	No rockburst	No rockburst

Fig. 17 Site survey photographs near the working face of each blasting cycle from September 18, 2018, to September 24, 2018

(a) 330th blasting cycle

(b) 331st blasting cycle

(c) 332nd blasting cycle

(d) 333rd blasting cycle

(e) 334th blasting cycle

(f) 335th blasting cycle

(g) 336th blasting cycle

(h) 337th blasting cycle

(i) 338th blasting cycle

(j) 339th blasting cycle

Verification in other engineering

In order to verify the rockburst time warning method proposed in this paper, further application and verification are carried out in the construction of another new railway tunnel. The tunnel is approximately 4900 m long, with a section shape of city gate type and a section size of 6.5 m × 6.5 m. The surrounding rock of the tunnel is trondhjemite, with a maximum burial depth of approximately 1800 m and a maximum principal stress of approximately 25 MPa in the horizontal direction. The tunnel was mainly excavated in whole sections using the D&B method. The average excavation step length is about 3.3 m, and the duration of a blasting cycle is approximately 12 h. To reduce the harm caused by rockburst, the method proposed in this paper has been adopted to carry out rockburst time warnings in the tunnel construction process since July 8, 2022. Among them, the rockburst warning results of 10 blasting cycles (recorded as the N77th to N86th blasting cycle) from August 5 to August 10, 2022, are shown in Fig. 18. If only the warning results of the first subsequent cycle are considered, in these 10 blasting cycles, a total of 1 moderate rockburst, 6 slight rockbursts, and 3 no rockburst were predicted. There were actually 6 slight rockbursts on site, so the rockburst warning accuracy is approximately 80.0% (8/10). Site survey photographs of one of the slight rockbursts are shown in Fig. 19. This field application once again proves that this rockburst time warning method has good engineering applicability.

Discussion

According to the analysis in "MSIPM," once the MSIPM is established, the predicted value of the MS information of the subsequent blasting cycle can be obtained by substituting
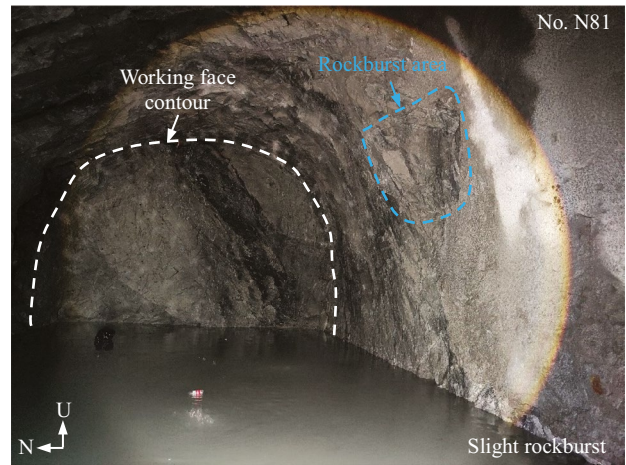

Fig. 19 Site survey photographs near the working face of the N81 blasting cycle

the MS information time series of the historical blasting cycle into the MSIPM. Therefore, after the predicted value of the MS information of the first subsequent blasting cycle is acquired, it is integrated into the MS information time series of the historical blasting cycle to form a new input vector. After the new input vector is substituted into the MSIPM, the predicted value of the MS information of the second subsequent blasting cycle can be determined. Theoretically, by continuously integrating the predicted values of the MS information of subsequent blasting cycles into the MS information time series of historical blasting cycles to establish a new input vector, the predicted values of the MS information of arbitrary future blasting cycles could be acquired. However, every time the predicted value of the MS information of one blasting cycle is incorporated, an

Fig. 18 Rockburst warning results of each blasting cycle of another new railway tunnel from August 5 to August 10, 2022, and the actual rockburst conditions on site

			No rockburst		Slight rockburst			Moderate rockburst			
Number of blasting cycle		N77	N78	N79	N80	N81	N82	N83	N84	N85	N86
Actual rockburst intensity		No	No	Slight	Slight	Slight	Slight	Slight	Slight	No	No
Warning results and release time (during the i-th blasting cycle)	N76	No		Slight	Slight						
	N77		Slight	Slight	Slight						
	N78			Slight	Slight	Slight					
	N79				Slight	Slight	Slight				
	N80					Slight	Slight	Slight			
	N81						Slight	Slight	Slight		
	N82							Slight	Moderate	Slight	
	N83								Moderate	Slight	No
	N84									No	
	N85										No

error is introduced, and with increasing error accumulation, the prediction effect increasingly deteriorates. Figure 10 and the analysis in "Establishment of the MSIPM" also verify this point. Therefore, to control the error, it is not suitable to apply the MSIPM to predict the MS information of more than three subsequent blasting cycles.

Similar to the MSIPM, once the RBTWM is established, theoretically, the intensity of potential rockbursts in arbitrary future blasting cycles can be forecasted. However, based on Fig. 13 and the Establishment of the RBTWM Section, the larger the interval between the warning and current blasting cycles is, the lower the rockburst warning accuracy becomes. Therefore, it is not suitable to apply the RBTWM to issue rockburst warnings related to more than three subsequent blasting cycles. Furthermore, the timing of potential rockburst in the next blasting cycle should be based on the most recent rockburst warning result.

Conclusion

Rockburst time warnings could provide an important reference for the accurate determination of the implementation timing of rockburst prevention and control measures. In this paper, the immediate rockbursts in tunnels excavated by the D&B method is selected as the research object, and the MSIPM and RBTWM based on LSTM are established by the deep learning method. In the process of building the model, various methods are applied to clean and correct the MS information and rockburst cases. With the MSIPM and RBTWM, the warning of immediate rockburst time is realized indirectly.

The MSIPM requires an input vector of the time series composed of the MS event number, energy, and apparent volume of historical blasting cycles and outputs the predicted values of the MS event number, energy, and apparent volume of subsequent blasting cycles. The predicted value is fused with the MS information of historical blasting cycles to establish the input vector of the RBTWM. In particular, the RBTWM requires the cumulative MS event number, energy, apparent volume, event rate, energy rate, apparent volume rate of historical blasting cycles, and the MS event number, energy, and apparent volume of subsequent blasting cycles as input vectors. The intensity of the potential rockburst of the subsequent blasting cycles is output as a vector. Thereby, the warning of the immediate rockburst time taking the blasting cycle as the unit is realized.

The above method has been applied in the construction of a railway tunnel excavated by the D&B method. The warning results of the test set in the application process demonstrate that the rockburst warning accuracy values for the first, second, and third subsequent blasting cycles are approximately 74.6%, 71.2%, and 63.1%, respectively. They

also demonstrate that the model has the best warning performance for moderate rockburst, followed by no rockburst. Further analysis indicates that larger intervals between the warning and current blasting cycles correlate with lower rockburst warning accuracy. Therefore, the intensity of the potential immediate rockburst in the next blasting cycle should be based on the latest rockburst warning result. In addition, further application and verification are carried out in the construction of another new railway tunnel. The rockburst warning accuracy for the first subsequent blasting cycles is approximately 80.0%. This field application once again proves that the rockburst time warning method has good engineering applicability.

Data availability The data that supports the findings of this study are available from the relevant author on the rational request.

Declarations

Conflict of interest The authors declare no competing interests.

References

Bi X, Zhang SN, Zhang Y, Hu L, Zhang W, Niu WJ, Yuan Y, Wang GW (2022) CASA-Net: a context-aware correlation convolutional network for scale-adaptive crack detection. Proceedings of the 31st ACM International Conference on Information and Knowledge Management, Atlanta, Georgia, USA, pp 67–76. https://doi.org/10.1145/3511808.3557252

Chawla NV, Bowyer KW, Hall LO, Kegelmeyer WP (2002) SMOTE: synthetic minority over-sampling technique. J Artif Intell Res 16:321–357. https://doi.org/10.1613/jair.953

Chen WZ, Lv SP, Guo XH, Qiao CJ (2009) Research on unloading confining pressure tests and rockburst criterion based on energy theory. Chin J Rock Mech Eng 28(08):1530–1540

Fajklewicz Z (2006) Rock-burst forecasting and genetic research in coal-mines by microgravity method. Geophys Prospect 31(5):748–765. https://doi.org/10.1111/j.1365-2478.1983.tb01083.x

Faradonbeh RS, Taheri A (2019) Long-term prediction of rockburst hazard in deep underground openings using three robust data mining techniques. Eng Comput 35(2):659–675. https://doi.org/10.1007/s00366-018-0624-4

Feng GL, Feng XT, Chen BR, Xiao YX, Yu Y (2015a) A microseismic method for dynamic warning of rockburst development processes in tunnels. Rock Mech Rock Eng 48:2061–2076. https://doi.org/10.1007/s00603-014-0689-3

Feng GL, Feng XT, Chen BR, Xiao YX (2015b) Microseismic sequences associated with rockbursts in the tunnels of the Jinping II hydropower station. Int J Rock Mech Min Sci 80:89–100. https://doi.org/10.1016/j.ijrmms.2015.06.011

Feng GL, Feng XT, Xiao YX, Yao ZB, Hu L, Niu WJ, Li T (2019a) Characteristic microseismicity during the development process of intermittent rockburst in a deep railway tunnel. Int J Rock Mech Min Sci 124:104135. https://doi.org/10.1016/j.ijrmms.2019.104135

Feng XT, Xiao YX, Feng GL, Yao ZB, Chen BR, Yang CX, Su GS (2019b) Study on the development process of rockbursts. Chin J Rock Mech Eng 38(4):649–673. https://doi.org/10.13722/j.cnki.jrme.2019.0103

Feng XT, Yang CX, Kong R, Zhao J, Zhou YY, Yao ZB, Hu L (2022) Excavation-induced deep hard rock fracturing: methodology and applications. J Rock Mech Geotech Eng 14:1–34. https://doi.org/10.1016/j.jrmge.2021.12.003

Gong FQ, Si XF, Li XB, Wang SY (2019a) Experimental investigation of strain rockburst in circular caverns under deep three-dimensional high-stress conditions. Rock Mech Rock Eng 52(5):1459–1474. https://doi.org/10.1007/s00603-018-1660-5

Gong FQ, Wu C, Luo S, Yan JY (2019b) Load–unload response ratio characteristics of rock materials and their application in prediction of rockburst proneness. Bull Eng Geol Environ 78(7):5445–5466. https://doi.org/10.1007/s10064-019-01474-6

Granter SR, Beck AH, Papke DJ Jr (2017) AlphaGo, deep learning, and the future of the human microscopist. Arch Pathol Lab Med 141(5):619–621. https://doi.org/10.5858/arpa.2016-0471-ED

Guo HS, Chen L, Zhu JY, Sun QC, Xiao YX (2022) Application of borehole camera technology in the identification of an instantaneous strain-structural-plane slip rockburst. Bull Eng Geol Environ 81(5):186. https://doi.org/10.1007/s10064-022-02658-3

Hatzor YH, He BG, Feng XT (2017) Scaling rockburst hazard using the DDA and GSI methods. Tunn Undergr Space Technol 70:343–362. https://doi.org/10.1016/j.tust.2017.09.010

He SQ, Song DZ, Li ZL, He XQ, Chen JQ, Li DH, Tian XH (2019) Precursor of spatio-temporal evolution law of MS and AE activities for rock burst warning in steeply inclined and extremely thick coal seams under caving mining conditions. Rock Mech Rock Eng 52(7):2415–2435. https://doi.org/10.1007/s00603-018-1690-z

Hoek E, Brown ET (1980) Underground excavations in rock. CRC Press, London

Hu L, Feng XT, Xiao YX, Feng GL, Li SJ, Pan PZ, Yao ZB (2019) Characteristics of the microseismicity resulting from the construction of a deeply-buried shaft. Tunn Undergr Space Technol 85:114–127. https://doi.org/10.1016/j.tust.2018.12.016

Hu L, Feng XT, Xiao YX, Wang R, Feng GL, Yao ZB, Niu WJ, Zhang W (2020) Effects of structural planes on rockburst position with respect to tunnel cross-sections: a case study involving a railway tunnel in China. Bull Eng Geol Environ 79(2):1061–1081. https://doi.org/10.1007/s10064-019-01593-0

Huang LQ, Li J, Hao H, Li XB (2018) Micro-seismic event detection and location in underground mines by using convolutional neural networks (CNN) and deep learning. Tunn Undergr Space Technol 81:265–276. https://doi.org/10.1016/j.tust.2018.07.006

Jiang Q, Feng X, Xiang T, Su G (2010) Rockburst characteristics and numerical simulation based on a new energy index: a case study of a tunnel at 2,500 m depth. Bull Eng Geol Environ 69(3):381–388. https://doi.org/10.1007/s10064-010-0275-1

Jiang Q, Zhang MZ, Yan F, Su GS, Feng XT, Xu DP, Feng GL (2021) Effect of initial minimum principal stress and unloading rate on the spalling and rockburst of marble: a true triaxial experiment investigation. Bull Eng Geol Environ 80(2):1617–1634. https://doi.org/10.1007/s10064-020-01995-5

LeCun Y, Bengio Y, Hinton G (2015) Deep learning. Nature 521:436–444. https://doi.org/10.1038/nature14539

Li XL, Wang EY, Li ZH, Liu ZT, Song DZ, Qiu LM (2016) Rock burst monitoring by integrated microseismic and electromagnetic radiation methods. Rock Mech Rock Eng 49(11):4393–4406. https://doi.org/10.1007/s00603-016-1037-6

Li TB, Ma CC, Zhu ML, Meng LB, Chen GQ (2017) Geomechanical types and mechanical analyses of rockbursts. Eng Geol 222:72–83. https://doi.org/10.1016/j.enggeo.2017.03.011

Liu JP, Feng XT, Li YH, Xu SD, Sheng Y (2013) Studies on temporal and spatial variation of microseismic activities in a deep metal mine. Int J Rock Mech Min Sci 60:171–179. https://doi.org/10.1016/j.ijrmms.2012.12.022

Liu GF, Jiang Q, Feng GL, Chen DF, Chen BR, Zhao ZN (2021) Microseismicity-based method for the dynamic estimation of the potential rockburst scale during tunnel excavation. Bull Eng Geol Environ 80(5):3605–3628. https://doi.org/10.1007/s10064-021-02173-x

Liu XQ, Wang G, Song LB, Han GS, Chen WZ, Chen H (2023) A new rockburst criterion of stress–strength ratio considering stress distribution of surrounding rock. Bull Eng Geol Environ 82(1):29. https://doi.org/10.1007/s10064-022-03042-x

Lu CP, Liu Y, Zhang N, Zhao TB, Wang HY (2018) In-situ and experimental investigations of rockburst precursor and prevention induced by fault slip. Int J Rock Mech Min Sci 108:86–95. https://doi.org/10.1016/j.ijrmms.2018.06.002

Luis RES, Tiago M, Rita LES, Joaquim T (2017) The use of data mining techniques in rockburst risk assessment. Engineering 3(4):552–558. https://doi.org/10.1016/J.ENG.2017.04.002

Martin CD (1997) Seventeenth Canadian geotechnical colloquium: the effect of cohesion loss and stress path on brittle rock strength. Can Geotech J 34(5):698–725. https://doi.org/10.1139/cgj-34-5-698

Mendecki AJ (1993) Keynote address: real time quantitative seismology in mines. Proceedings of third international symposium on rock-bursts and seismicity in mines. Kingston, Ontario, Canada, pp 287–295

Meng FZ, Zhou H, Wang ZQ, Zhang LM, Kong L, Li SJ, Zhang CQ, Hu SC (2017) Experimental study of factors affecting fault slip rockbursts in deeply buried hard rock tunnels. Bull Eng Geol Environ 76(3):1167–1182. https://doi.org/10.1007/s10064-016-0926-y

Mitri HS (2007) Assessment of horizontal pillar burst in deep hard rock mines. Int J Risk Assess Manag 7(5):695–707. https://doi.org/10.1504/IJRAM.2007.014094

Müller W (1991) Numerical simulation of rock bursts. Min Sci Technol 12(1):27–42. https://doi.org/10.1016/0167-9031(91)91513-H

Ortlepp WD (2005) RaSiM comes of age-a review of the contribution to the understanding and control of mine rockburst. Proceeding of the 6th International Symposium on Rockburst and Seismicity in Mines. Australian, Nedlands, pp 3–20

Pu YY, Apel DB, Xu HW (2019) Rockburst prediction in kimberlite with unsupervised learning method and support vector classifier. Tunn Undergr Space Technol 90:12–18. https://doi.org/10.1016/j.tust.2019.04.019

Shi XZ, Zhou J, Dong L, Hu HY, Wang HY, Chen SR (2010) Application of unascertained measurement model to prediction of classification of rockburst intensity. Chin J Rock Mech Eng 29(S1):2720–2726

Singh SP (1987) The influence of rock properties on the occurrence and control of rockbursts. Min Sci Technol 5(1):11–18. https://doi.org/10.1016/S0167-9031(87)90854-1

Stacey TR (2013) Dynamic rock failure and its containment. Proceedings of the First International Conference on Rock Dynamics and Applications, Lausanne, Switzerland, pp 57–70

Vacek J, Chocholoušová J (2008) Rock burst mechanics: insight from physical and mathematical modelling. Acta Polytech 48(6):38–44. https://doi.org/10.14311/1071

Wang JA, Park HD (2001) Comprehensive prediction of rockburst based on analysis of strain energy in rocks. Tunn Undergr Space

Technol 16(1):49–57. https://doi.org/10.1016/S0886-7798(01)00030-X

Xiao YX, Feng XT, Hudson JA, Chen BR, Feng GL, Liu JP (2016) ISRM suggested method for in situ microseismic monitoring of the fracturing process in rock masses. Rock Mech Rock Eng 49(1):343–369. https://doi.org/10.1007/s00603-015-0859-y

Zhang Y, Feng XT, Zhang XW, Wang ZF, Sharifzadeh M, Yang CX, Kong R, Zhao J (2019) Strain energy evolution characteristics and mechanisms of hard rocks under true triaxial compression. Eng Geol 260:105222. https://doi.org/10.1016/j.enggeo.2019.105222

Zhang W, Feng XT, Bi X, Yao ZB, Xiao YX, Hu L, Niu WJ, Feng GL (2021) An arrival time picker for microseismic rock fracturing waveforms and its quality control for automatic localization in tunnels. Comput Geotech 135:104175. https://doi.org/10.1016/j.compgeo.2021.104175

Zhao TB, Yin YC, Xiao FK, Tan YL, Zou JC (2014) Rockburst disaster prediction of isolated coal pillar by electromagnetic radiation based on frictional effect. Sci World J 2014:1–7. https://doi.org/10.1155/2014/814050

Zhao GB, Wang DY, Gao B, Wang SJ (2017) Modifying rock burst criteria based on observations in a division tunnel. Eng Geol 216:153–160. https://doi.org/10.1016/j.enggeo.2016.11.014

Zhou KP, Gu DS (2004) Application of GIS-based neural network with fuzzy self-organization to assessment of rockburst tendency. Chin J Rock Mech Eng 23(18):3093–3097

Zhou J, Li XB, Mitri HS (2018) Evaluation method of rockburst: state-of-the-art literature review. Tunn Undergr Space Technol 81:632–659. https://doi.org/10.1016/j.tust.2018.08.029

Zhu WC, Li ZH, Zhu L, Tang CA (2010) Numerical simulation on rockburst of underground opening triggered by dynamic disturbance. Tunn Undergr Space Technol 25(5):587–599. https://doi.org/10.1016/j.tust.2010.04.004

Zubelewicz A, Mroz Z (1983) Numerical simulation of rock burst processes treated as problems of dynamic instability. Rock Mech Rock Eng 16(4):253–274. https://doi.org/10.1007/BF01042360